Macromolecules

Article

Cite This: Macromolecules 2018, 51, 4865−4873

Crystal Growth in Polyethylene by Molecular Dynamics: The Crystal Edge and Lamellar Thickness

Tuukka Verho,* Antti Paajanen, Jukka Vaari, and Anssi Laukkanen

VTT Technical Research Centre of Finland Ltd., Espoo, Finland

ABSTRACT: We carried out large-scale atomistic molecular dynamics simulations to study the growth of twin lamellar crystals of polyethylene initiated by small crystal seeds. By examining the size distribution of the stems—straight crystalline polymer segments—we show that the crystal edge has a parabolic profile. At the growth front, there is a layer of stems too short to be stable, and new stable stems are formed within this layer, leading to crystal growth. Away from the edge, the lengthening of the stems is limited by a lack of available slack length in the chains. This frustration can be relieved by mobile crystal defects that allow topological relaxation by traversing through the crystal. The results shed light on the process of polymer crystal growth and help explain initial thickness selection and lamellar thickening.

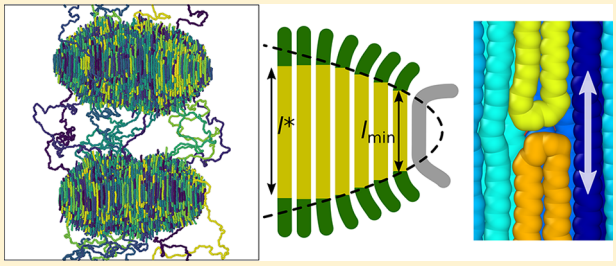

INTRODUCTION

Most commodity and engineering plastics are semicrystalline, which means that their macroscopic properties strongly depend on the shape, size, and connectivity of the constituent microscopic crystallites.[1−3] Therefore, understanding the process of polymer crystallization is key to understanding and controlling the properties of this technologically important group of materials. However, the length of the polymer chains and the entanglements between them make polymer crystallization a complex and kinetically controlled process.[4−6] Challenges in complete experimental characterization, theoretical description, and computer simulations of polymers still limit our understanding of this basic aspect of polymeric materials.

Because of the limitations in available experimental methods, the molecular level kinetic mechanism of the growth of polymer crystals is still a subject of speculation.[7,8] Even though the large interfacial energy associated with the fold surface (where chains exit and enter the crystal) would thermodynamically favor thick extended-chain crystals, polymers are found to form thin folded lamellae only 10 or more nanometers thick. In these lamellae, the chains make a large number of folds that, although increase the free energy, make crystallization more kinetically accessible. The crystal grows by addition of new straight chain segments—stems—onto its growth face. A number of theoretical models have been suggested to describe this process. More recently, computer simulations have started to shed light on the molecular level dynamics.

The Lauritzen−Hoffman (LH) theory has been widely employed as a model for polymer crystal growth.[9,10] The rate-limiting step in the model is the attachment of a stem on a flat crystal surface, followed by attachment of more stems next to it to complete a new layer of stems. The length of the new stem is assumed to equal the thickness of the lamella, which causes the growth of thicker lamellae to have a larger kinetic barrier, leading to the conclusion that only thin lamellae grow fast. However, thermodynamics dictates a minimum thickness $l_c(T)$ for the lamella, as the heat of fusion should offset the free energy cost caused by the fold surface. The observed lamellar thicknesses are slightly above this thermodynamic minimum.[11]

Sadler and Gilmer questioned the assumption in the LH theory that the length of stems at the growth edge is equal to the thickness of the lamella.[12] Indeed, recent simulations suggest that newly attached stems tend to be shorter than ones inside the crystal.[13−16] Sadler and Gilmer formulated a model (the SG model) for crystal growth based on rate constants for the attachment and detachment of new stems and their subsequent growth or shortening.[17,18] In this model, new stems at the growth front are initially small but can gradually increase their size. However, the stems can grow only as long as they are at the growth front, i.e., until new stems cover them—although the growth can resume if the stem is exposed again due to the dissociation of the covering stems. Yet, in simulations of crystal growth in polyethylene, stems grow in length also behind the growth front due to the translational mobility of crystalline chains, contrary to the assumptions in the SG model.[13,16] Polyethylene and several other polymers have been found to exhibit lamellar thickening after crystallization when kept close to their melting temperature.[4] This indicates that chain mobility within the crystal allows reorganization of the polymer chains and increasing of the stem length within the crystal. In simulations, particularly fast lengthening has been observed near the growth front at the edge of the crystal, which has a tapered or wedge-shaped profile.[13,14,16] Jiang et al.[16] proposed a model for crystal growth where the inverse growth rate is a sum of two characteristic

Received: April 24, 2018
Revised: June 14, 2018
Published: June 28, 2018

DOI: 10.1021/acs.macromol.8b00857
Macromolecules 2018, 51, 4865−4873

times, the nucleation time for attachment of a new stem, and the time it takes for a new stem to grow to the full thickness of the lamella.

Several groups have performed numerous molecular dynamics (MD) studies on polymer crystal nucleation and growth. Luo, Sommer, and co-workers have employed a coarse-grained model of poly(vinyl alcohol) to study various aspects of crystallization, with a particular emphasis on the influence of entanglements and memory effects.[13,19−27] The largest system studied was a self-seeded crystal lamella in a system of a million repeat units. Yamamoto and co-workers have performed melt crystallization simulations with a coarse-grained polymer model.[14,28−33] In the largest simulation with approximately 130 000 repeat units, the growth of polymer crystal on a substrate was studied. Rutledge and co-workers have simulated the nucleation and growth of crystals in oriented polyethylene melts using the united-atom force field by Paul et al.[34] with some modifications.[35−39] They have also developed a Monte Carlo method to prepare the amorphous interlamellar phase and used it to study mechanical deformation and other properties.[38,40−44] Muthukumar and co-workers simulated polymer crystal nucleation in solution with a united-atom force field.[45−50] Gee and Lacevic studied the rapid crystallization of stiffened polymers in large systems of up to 5 million united atoms (UAs).[51,52] Because of computational costs, all molecular dynamics simulations are limited to very short time scales, and only the deep undercooling regime can be studied with the method. However, Hu and co-workers used the kinetic Monte Carlo lattice method to study the growth of polymer crystals and could access other dynamic regimes.[15,16,53−58] Karayiannis and co-workers have studied the crystallization of freely jointed hard sphere polymers with an off-lattice kinetic Monte Carlo approach.[59−62]

In this work, we perform large-scale MD simulations of the formation of crystal lamellae in polyethylene in a system containing 3 million UAs (CH_2 or CH_3 units) in 3000 polymer chains, with simulation times exceeding 1 μs. The number, position, and orientation of the crystals are controlled with short immobilized seed chains. We grow two lamellae simultaneously to observe the formation of tie segments between the crystals. The large system size and long simulation time combined with a realistic force field give new understanding of the crystallization process. The crystal can be divided into an edge region of 2−3 nm where the growth process of the crystal takes place and a central region with slowly increasing thickness that represents a bulk crystal. In the edge region, we learn about the shape and the attachment of new stems at the growth front, while in the central region, we observe arrested thickening due to the lack of available slack length and mobile defects that allow topological relaxation.

COMPUTATIONAL METHODS

Molecular Dynamics. MD simulations of polyethylene crystallization were performed with the GROMACS package.[63] The temperature of the simulation was controlled with the velocity rescaling algorithm, and the pressure of the periodic simulation box was maintained at zero with the Berendsen barostat. The velocity-Verlet algorithm was used for time integration with a time step of 4 fs.

The force field parameters were taken from Ramos et al.[64] The parameters follow the TraPPE-UA values,[65] except that bonds are described by a harmonic potential instead of stiff constraints. Additionally, Ramos et al. had a slight deviation from TraPPE-UA in the torsion force parameters, such that the energy difference between the *gauche* and *trans* conformations is 0.83 kcal/mol versus the value 0.77 kcal/mol in TraPPE-UA. This slightly favors straight conformations, accelerating crystallization. To avoid making the density of the system sensitive to the cutoff value for the Lennard-Jones interactions, we applied long-range energy and pressure corrections, as indicated in Martin and Siepmann.[65] For the cutoff, we used a value of 1.0 nm.

Generation of Equilibrated Initial States. The chain-level relaxation of chains of 1000 UAs is extremely slow in MD time scales. To generate an equilibrated starting configuration, we applied the following procedure. First, to prepare initial conformations for the chains, we used a random walk modeled as a Markov process. The probabilities for the sequences *trans*−*gauche*, *trans*−*trans*, and *gauche*$^+$−*gauche*$^-$ were obtained from short MD simulations on small systems at a reference temperature of 400 K, and the random walk was performed based on the obtained probabilities. The resulting chains were placed in a periodic box, and their packing was subsequently optimized to minimize density fluctuations following Auhl et al.[66] A number of rigid-body Monte Carlo moves (translation, rotation, reflection, inversion, exchange) were performed to the chains to progressively reduce the variance of density within the system. An MD simulation with capped Lennard-Jones interactions was then performed to slowly introduce excluded volume interactions while maintaining the overall conformations of the chains. The capping was performed by defining an interaction distance below which the force no longer increases. The cap was initially at 0.8σ, where σ is the equilibrium separation distance for the force. The capped interaction was turned on gradually over a time interval of 360 ps by applying a prefactor that increases from 0.1 to 1. The purpose of this was to remove overlaps with the crystal seeds. Thereafter, the cap was gradually removed over a simulation time of 80 ps, after which normal MD simulation could proceed.

Heterogeneous Crystallization from a Crystal Seed. To initiate crystallization in a controlled manner, two crystal seeds were placed in the simulation box. These seeds consisted of 4 short polymer chains of 40 UAs placed in a formation according to the crystal structure of polyethylene. The particles were fixed in place with a harmonic potential with a force constant of 5000 kJ/(mol nm^2). Overlaps between the seed chains and the polymer chains in the initial configuration were removed during the push-off phase (see above).

Identification of Crystalline Regions. Polymer crystals were considered as aggregates of stems, which are straight polymer segments. The local direction of the polymer chain is given by the chord vector $\mathbf{d}_n = (\mathbf{r}_{n+1} - \mathbf{r}_{n-1})/|\mathbf{r}_{n+1} - \mathbf{r}_{n-1}|$. We can define an order parameter λ for a segment of length $2k + 1$ by

$$\lambda = \frac{1}{2k+1} \sum_{i=-k}^{k} \mathbf{d}_{n+i} \cdot \mathbf{d}_n^{\mathrm{av}} \tag{1}$$

where $\mathbf{d}_n^{\mathrm{av}}$ is the average chord direction within the segment. λ represents the average deviation of the chords from the overall direction of the chain. Equation 1 can be simplified to

$$\lambda = \frac{1}{2k+1} \left| \sum_{i=-k}^{k} \mathbf{d}_{n+i} \right| \tag{2}$$

DOI: 10.1021/acs.macromol.8b00857
Macromolecules 2018, 51, 4865−4873

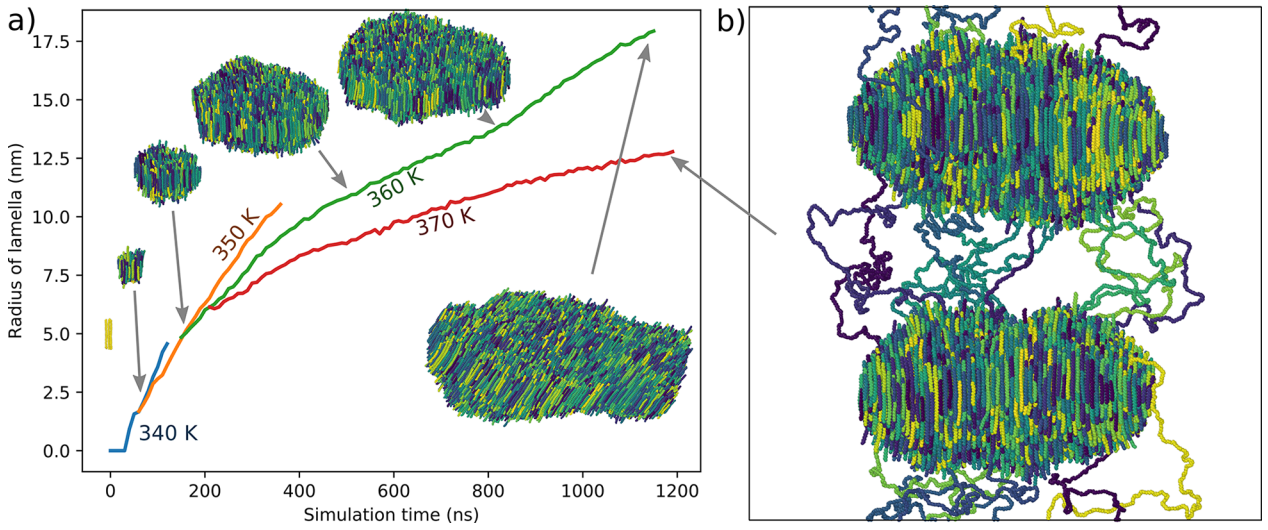

Figure 1. Growth of a polyethylene crystal lamella. (a) Crystal growth is initiated from seeds at 340 K, after which temperature is progressively increased. One of the crystal lamellae is shown at different stages of growth. (b) The two lamellae and connecting tie segments at t = 1200 ns.

If λ at n exceeds a threshold value (0.9), the segment from $n - k$ to $n + k$ is considered straight. We used k = 7, i.e., the minimum length of a stem is 15 repeat units, or k = 5 when information about very short stems was desired. Several overlapping straight segments obviously form one long stem.

In previous literature, a hard limit for the angle between consecutive chords or a order parameter based on the squared dot product of chords has been used. We chose the present criterion because it is less sensitive to local chord angle fluctuations that do not change the overall direction of the segment than to those that do change it. A lower value of the threshold for λ would effectively move the interface between the crystalline and amorphous phase slightly toward the amorphous side, as larger deviations in the chord orientations would be allowed. A higher value would cause stems to be more easily split in two due to temporary defects, although that would not be a major issue when the whole lifetime of the stem is analyzed.

To track the evolution of stems during the simulation, we calculated λ values for simulation frames every nanosecond. The analysis was then performed in (n, t) space for each chain, such that a continuous region with λ above the threshold constitute the lifespan of one stem.

RESULTS AND DISCUSSION

Growth of the Crystals. The crystals were grown from amorphous melt that contains two crystal seeds of four oligomeric chains. The starting temperature for crystallization was 340 K, where crystals started to grow within tens of nanoseconds. However, homogeneous nucleation would also soon start to take place in addition to the growth around the seeds, so the temperature needed to be increased to 350 K after 60 ns to melt away any homogeneously nucleated crystal nuclei. Crystal growth was then studied at 350, 360, and 370 K. As shown in Figure 1a, the simulations at different temperatures were realized as "branches" from an ongoing simulation at lower temperature, such that the previous simulation provided an initial state with thermodynamically stable nuclei.[20,38] The size of the lamella is expressed by its radius $R = (n_{stems}A_s/\pi)^{1/2}$, where n_{stems} is the number of stems in the lamella and A_s is the area taken by one stem. Figure 1b shows the two lamellae with all amorphous segments except tie segments removed. The size of the simulation box was approximately 44 nm, so the distance between the centers of the lamellae was 22 nm. The amorphous layer between the lamellae ended up being roughly 10 nm thick.

Tapered Shape and Attachment of New Stems. Figure 2 shows a stem length map of the crystals at 370 K after 1200 ns of simulation. The average thickness of the lamellae in the central region is approximately 12 nm (90−100 UAs), although the length of the stems varies between 70 and 120 UAs. In the edge region, less than 3 nm from the growth front, the stems are shorter and undergoing relatively fast growth.

As shown by the varying distances between the "growth rings" in Figure 2, the growth rate of the crystal has large spatial and temporal variations. Surprisingly, however, this does not lead to variation in the stem length profile in the edge region; instead, the crystal has a uniform tapered shape throughout its perimeter. Furthermore, this shape does not change during the simulation, as shown below.

To quantify the shape of the edge, we calculated the stem length distribution of the crystals at different stages of the simulation. Figure 3a shows the evolution of the distribution for one crystal at 370 K. Interestingly, the distribution has a constant slope at lower stem lengths (below 8 nm) that follows a straight line with $\phi(l) = c_0 l/R$, where c_0 = 0.13 nm^{-1}. This linear relationship holds for all of our data at different temperatures. Evidently, the shape of the edge is such that it results in a linear stem length distribution. Using ds to denote the distance over which the stem length increases by dl, we can write (assuming a circular cross section for the crystal):

$$2\pi(R - s)\mathrm{d}s = \pi R^2 \phi(l)\mathrm{d}l \tag{3}$$

where s is the distance from the growth front. Note that the stem length distribution has units of length^{-1}. The left side of the equation is the area of a circular band of thickness ds and radius $R - s$. The right side is the area of the crystal taken by stems with length between l and l + dl. This gives us a differential equation

$$\frac{\mathrm{d}l}{\mathrm{d}s} = \frac{2(R - s)}{R^2 \phi(l)} \tag{4}$$

DOI: 10.1021/acs.macromol.8b00857
Macromolecules 2018, 51, 4865−4873

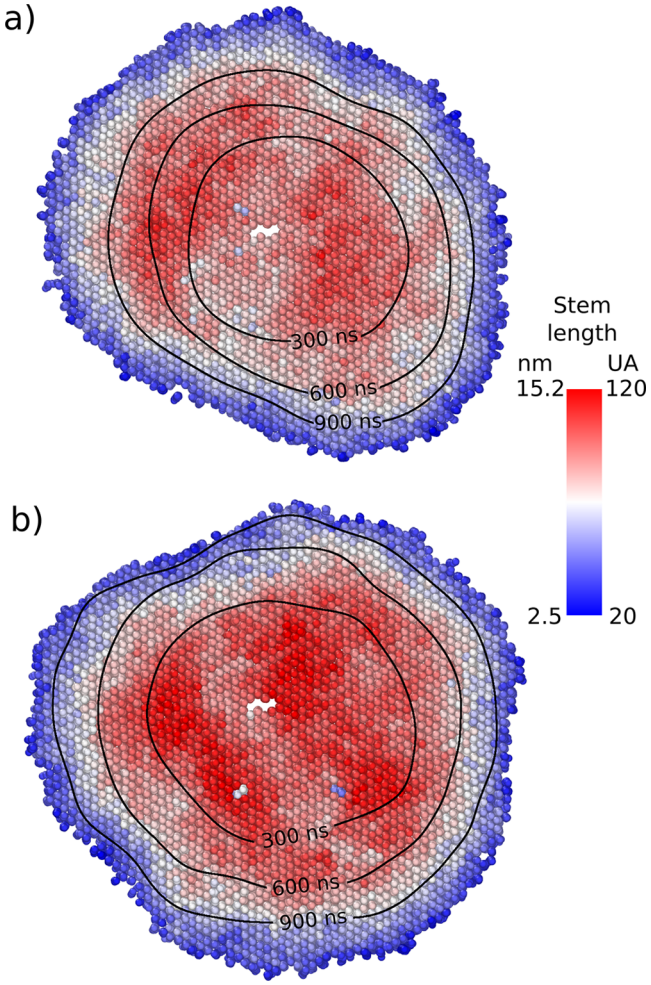

Figure 2. Cross sections of the two lamellae at 370 K, t = 1200 ns. The stems are colored by their length, showing the thickness profile. Only long-lived stems are shown. The holes inside the crystals show the position of the seed chains, which are omitted from the visualization. Earlier grain perimeters at 300, 600, and 900 ns are show as "growth rings".

For a large lamella with $R \gg s$, we can simplify

$$\frac{dl}{ds} = \frac{2}{R\phi(l)} \tag{5}$$

With $\phi(l) = c_0\, l/R$, the profile is parabolic

$$l = 2\sqrt{\frac{s}{c_0}} \tag{6}$$

For a finite R, the solution is an elliptical profile $l \sim \sqrt{s(2R - s)}$. Therefore, the crystal is initially roughly an ellipsoid, but as it grows, its middle section becomes flattened due to hindered thickening (discussed further below) and the profile of the edge eventually becomes parabolic.

The smallest stems that form at the growth front are not stable but tend to have short lifetimes. Only when they grow large enough as a result of a fluctuation, they stabilize and start to grow steadily. Figure 3b shows a typical plot of average stem growth rates as a function of stem length. There is a clear turning point $l = l_{min}$ at the length of approximately 4 nm when stems start to grow rather than shrink on average, indicating a critical size when the stem becomes thermodynamically stable.

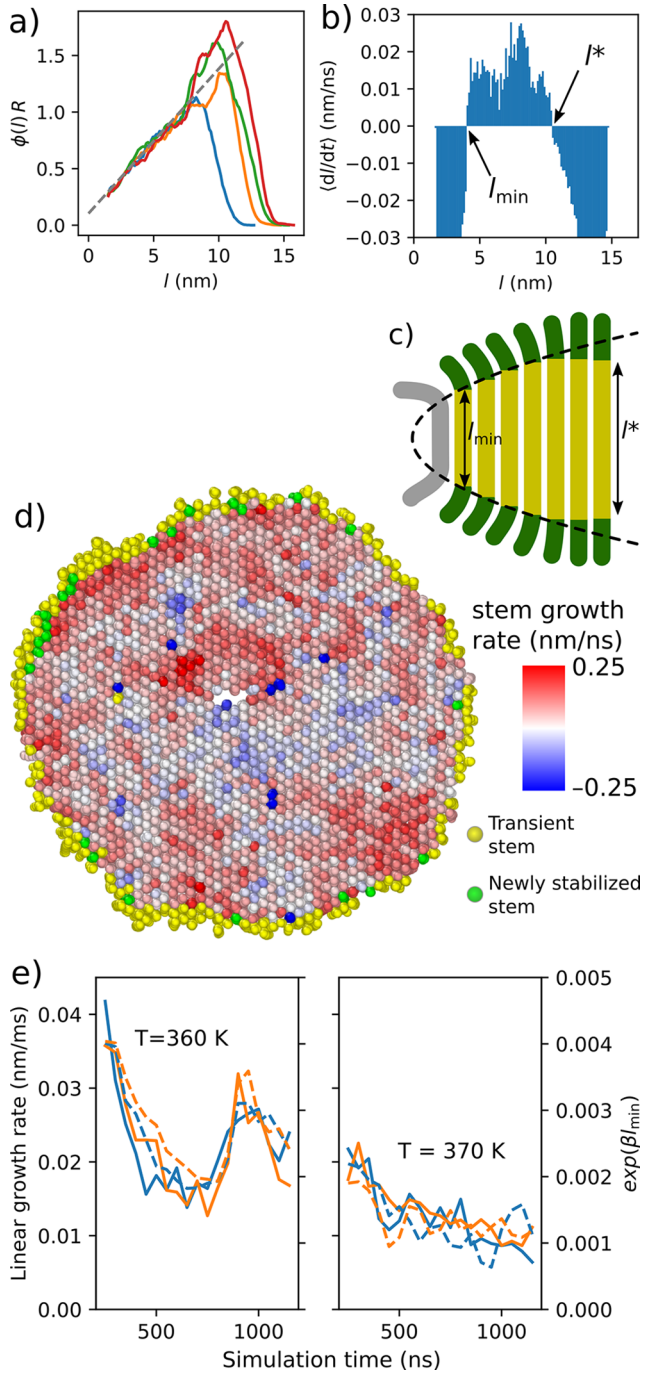

Figure 3. Shape of the edge and growth of stems. (a) The stem size distribution $\phi(l)$ scaled by lamellar radius. The plots are for t = 300, 600, 900, and 1200 ns. (b) The average stem growth rate as a function of stem length. Note that deviations from the average are prevalent, so stems of any size can grow or shrink. (c) A schematic of the parabolically shaped edge region. (d) The cross section of a lamella at 370 K, t = 650 ns. Stems that have not reached the size l_{min} are shown in yellow (only stems at least 1.9 nm long are shown) and ones that have just reached l_{min} in green. Other stems are colored by growth rate averaged over 80 ns. (e) The growth rate of the radius of the two lamellae (solid lines) and the exponential $\exp(\beta l_{min})$ (dashed lines) where the parameter β = 0.48. The two colors represent the two lamellae. The left and right plots show the 360 and 370 K simulations, respectively.

Likewise, there is a turning point at the length $l = l^*$ above which the stems are more likely to shrink than grow. l^* can be

DOI: 10.1021/acs.macromol.8b00857
Macromolecules 2018, 51, 4865−4873

interpreted as the thickness of the lamella. Another way to determine the thickness is the peak of the stem length distribution—Figure 3a shows the gradual shift of the peak to higher values during the simulation.

Reaching the critical size l_{min} is a requirement for a stem's survival and represents a basic step of lamellar growth. Stems with size below l_{min} exist only as thermal fluctuations and are mostly short-lived. We consider the growth front to be where the thickness of the lamella is l_{min}, such that it is the interface between stable, crystalline stems and unstable, transient stems. Interestingly, the growth front is not apparent in the thickness profile of the edge, as the transient stems still follow the parabolic profile, as shown schematically in Figure 3c. Although the transient stems are short-lived, new ones are constantly forming from the melt and exist constantly on the growth front, as shown in Figure 3d. The stems that reach the size l_{min} and become attached to the crystal (shown with green color in Figure 3d) are therefore surrounded by other stems, stable or unstable. After reaching a stable size, the stems undergo fluctuating growth in correlated domains of roughly 4 nm, as can be seen in Figure 3d. There seems to be some correlation between local stem growth and addition of new stable stems at the growth front, which is in accord with the observation that the profile of the edge is conserved.

l_{min} is the size at which a stem is not inclined to either shrink or grow, implying the stem is in a certain kind of equilibrium with its environment. To reach this size, the segment needs to cross an entropic barrier. We found the value of l_{min} to depend on temperature: the approximate values were 3.1, 3.6, and 4.1 nm at 350, 360, and 370 K, respectively. However, these are only typical values, as l_{min} was not completely constant during the simulations but varied in correlation with the growth rate of the crystal. Figure 3e plots the growth rate of the lamellar radius as a function of time, as well as the exponential $\exp(\beta l_{min})$, where β is a fitting parameter. The two plots overlap, suggesting that the free energy barrier for attachment of new stems is related to l_{min}.

Chain Crystallinity and Topological Relaxation. Insight into the formation and growth of stems within chains can be obtained by looking at trajectories of individual chains. Figure 4a shows how a chain gradually becomes entirely embedded in a crystal. The stems often attach in pairs, forming tight folds. The reason for this is that the formation of a stem within an amorphous chains segment stretches it locally, causing another straight segment to form to compensate, which tends to become a stem as well (see the t = 310 ns and t = 410 ns snapshots in Figure 4a). When the stems grow, they need slack length from the amorphous parts to be transferred to them. This often proceeds by diffusion through other stems. In polyethylene, axial translation in the crystalline phase is relatively easy—an α-relaxation process has been identified in crystalline polyethylene, which facilitates pulling chains through the crystal.[4]

Eventually, essentially the whole polymer chain becomes a part of the crystal. At this point, further lengthening of stems is not possible without reducing the number of stems. Consequently, the thickening of the crystal lamella within the area occupied by the chain will become hindered. Figure 4c shows the crystallinity of chains within a lamella. From the figure, one can notice that stems close to the edge tend to belong to chains with relatively low crystallinity. However, in the central region, many chains are essentially fully crystalline and therefore do not have available slack length (some 10–

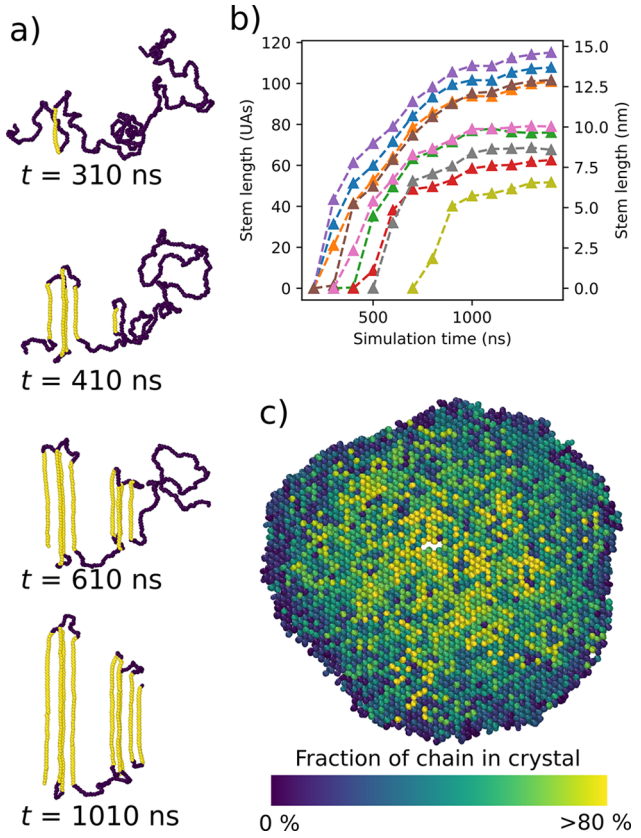

Figure 4. Crystallization of chains. (a) Snapshots from the trajectory of a chain that eventually becomes completely embedded in a crystal. Crystalline stems are shown in yellow. (b) The growth of stems in the chain shown in (a). (c) Stems in a crystal colored by the crystalline fraction of the chain they belong to.

20% of residual amorphous material is always needed to accommodate folds and loops). When the density of chains that can no more grow their stems becomes sufficiently high, the thickening of the crystal will cease.

To remove blocks for further thickening, a simple way for a chain to reduce the number of its stems would be to pull a chain end through the crystal. However, this would introduce a line defect that would resist the diffusion of the chain end, causing a barrier that grows with the thickness of the crystal. As it turns out, there is a much easier way for the chain to achieve the same. We found a previously unreported type of mobile defect that allows a fold or a chain end to be pulled through the crystal without the need for an energetically costly line defect, effectively resulting in topological relaxation (altering the connectivity between stems). Figure 5a shows a *fold-against-fold* defect, which allows a tight fold (hairpin) to be pulled out of the crystal and be replaced by another. The way the other fold pushes into the crystal through the fold surface is similar to what was reported by Yamamoto,[14] but the role of another fold receding from the crystal has not been mentioned before. The cooperative nature of the formation and movement of the defect is crucial because it avoids the introduction of a line defect. Notably, this defect does not require any chain ends to be present. Another type of defect that does require the presence of chain ends is shown in Figure 5b. This one allows a chain end to be pulled through the crystal and be replaced with another. However, this *end-against-end* defect is expected to be far less common than the

DOI: 10.1021/acs.macromol.8b00857
Macromolecules 2018, 51, 4865–4873

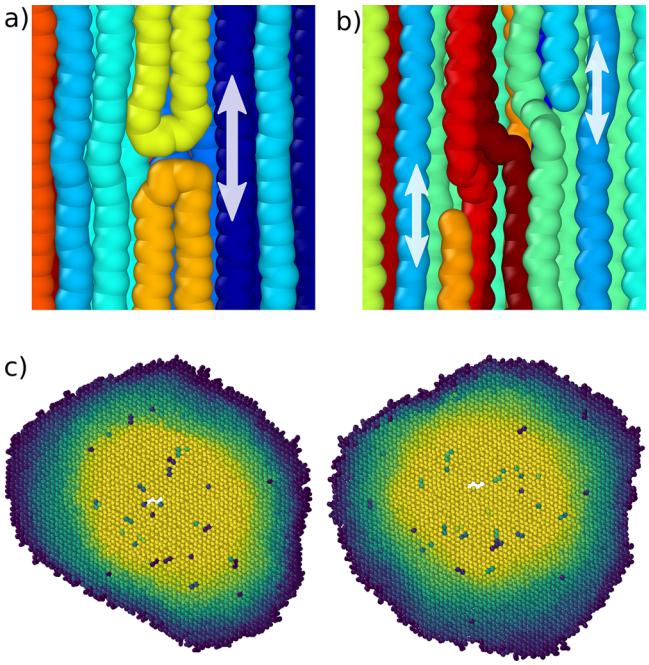

Figure 5. Mobile crystal defects that allow topological reordering. (a) A fold (orange chain) is pulled through the lamella and replaced by another (yellow chain). (b) A complex defect where the orange chain end is being pulled through the crystal and the light blue chain is being incorporated in the crystal. The other chains make kinks that allow the light blue end to enter the crystal at a different location than the original orange stem. A simpler version of this defect, where the two chain ends are head-to-head without other chains involved, was also witnessed, but less often. (c) The cross sections of the lamellae colored by stem age at 370 K at t = 1500 ns. Younger stems inside the crystal indicate that older stems have been replaced by the mechanisms shown in (a) and (b).

fold-against-fold defect in high molecular weight polymers with a low density of chain ends. It is possible for an amorphous chain to enter the crystal in these ways; in our case, however, those were exceptions, as the folds and chain ends entering the crystal mostly came from partially crystalline chains.

A relatively large number of stems were replaced by new ones during the simulation. Figure 5c shows the crystal cross sections colored by stem age, clearly showing a number of stems significantly younger than their surrounding. Pairs of younger stems are usually a result of the fold-against-fold defect propagating through the crystal (Figure 5a) whereas isolated younger stems originate from end-against-end defects.

Chain Tilt. A varying degree of chain tilt—angle between the stem axes and the normal of the lamella—has been commonly observed in experiments (typically ≈35°).[41] Here, the initial growth around the seed chains took place without tilt. However, when the lamella grew large enough at 360 K, a tilt of approximately 45° developed rather suddenly, as shown in Figure 6. The seed chains were still constrained to be aligned toward the z direction, so the tilting required the formation of a significant crystal defect around the seed, which demonstrates the thermodynamic driving force for it. This force is believed to arise from a more advantageous packing of chains exiting the crystal.[41] Without the seed chains the tilting would be expected to happen earlier, which we confirmed to happen with a test simulation where the seed was removed at 370 K at t = 1000 ns. The tilting of the chains was accompanied by a temporary increase in the rate of crystal

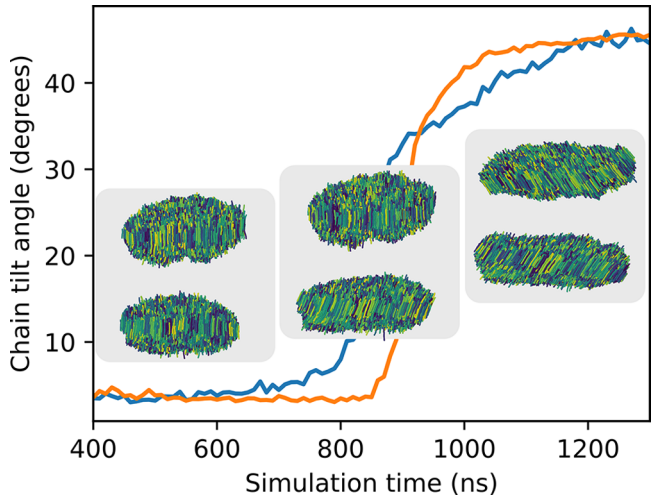

Figure 6. Development of the tilt angle at 360 K.

growth at 360 K as shown in Figures 1a and 3e. A chain tilt was also observed by Luo and Sommer in their simulation of the growth of a single lamella.[13]

Loops, Tails, and Tie Segments. The nature of the fold surface has been a topic of debate among researchers. The main question is whether the fold surface is dominated by tight folds connecting adjacent stems or whether the surface rather resembles a "random switchboard". Here, the fraction of both nearest-neighbor and next-nearest-neighbor re-entries was 24%, so the fraction of tight folds was therefore 48%. The fraction is somewhat lower than the value 58% reported by Yamamoto.[14] DiMarzio and Guttman argued, based on random walk statistics, that the fraction of tight folds should be at least approximately 2/3. However, the loops in our simulation did not follow random-walk statistics at all. Rather, due to the reeling effect of growing stems as described above, the loops were progressively pulled tight to maximize the amount of length available for the stems. Furthermore, over 10% of stems ended with tails of negligible length that contribute little to the density of the interfacial layer. The fraction of tie segments (that connect the two lamellae) of all stem-to-stem connections was approximately 0.4%. This low number is likely to be a consequence of the relatively short length of the polymer chains (M_w = 14 kDa) compared to what is typically used in high-density polyethylene products.

Tight folds typically form when two stems form in pairs, as can be seen in Figure 4a. Occasionally, even triplets or longer sequences of stems form consecutive tight folds. Here, the fractions of 1, 2, 3, and >3 consecutive folds were 74%, 18%, 6%, and 2%, respectively.

Not only loops were pulled tight by the reeling forces caused by growing stems, but tail and tie segments as well. Figure 7 plots the mean-squared internal displacement $\langle R^2 \rangle(|n - m|)$ divided by $|n - m|$ for completely amorphous chains, tail segments, and tie segments, depicting intrachain distances as a function of the separation of monomers. Tail segments clearly deviate from the random-chain statistics of the amorphous chains due to the reeling effect that increases distances with intermediate to large monomer separations. With tie segments, the effect is doubled because in their case the pulling is applied at both ends.

DOI: 10.1021/acs.macromol.8b00857
Macromolecules 2018, 51, 4865−4873

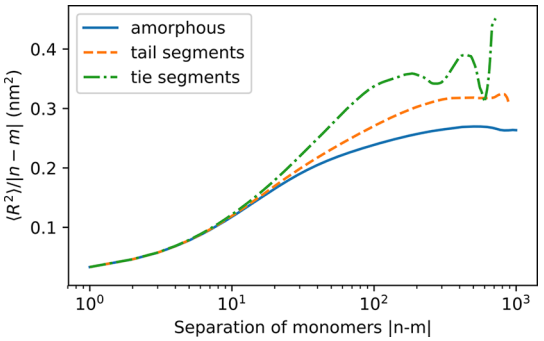

Figure 7. Mean-squared internal distances for completely amorphous chains, tails segments, and tie segments at 370 K and t = 1200 ns.

DISCUSSION

Attachment of new stems and their subsequent lengthening within the edge region are central to the growth of crystals of polyethylene and other polymers with chain mobility in the crystalline phase. Jiang et al.[16] as well as Luo and Sommer[13] suggested that the lengthening of newly attached stems is governed by a kinetic barrier that depends on the length of the stem, leading to logarithmic growth. However, this would imply that the profile of the edge results from the relative rates of stem attachment and their subsequent growth. If these rates were independent, spatial and temporal variations in the rate of attachment of new stems would lead to variations in the profile of the edge: a steep profile at slowly growing fronts and a more gradually thickening profile at rapidly growing fronts. Instead, we showed that the profile has a constant parabolic shape that does not seem to be affected by the interplay of stem attachment and lengthening. In fact, the opposite seems to be the case: the relative attachment and lengthening rates are determined so that the shape is conserved. Therefore, the shape of the edge is kinetically stable, as previously suggested by Yamamoto based on the observation that the tapered shape was retained during melting.[14]

For a possible explanation for this stable parabolic shape, we invoke the same concept that has been used to explain chain tilt in polymer crystals. The tilt allows more favorable arrangement of folds and chain segments exiting the crystal at the fold surface, alleviating the density anomaly at the interfacial layer and reducing the associated loss of entropy.[41] An effective tilt is also achieved by the tapered shape because the chains are not parallel to the normal of the fold surface, as shown in Figure 3c. This entropy gain might be enough to stabilize the configuration, so that as new stems are incorporated, the previously attached ones grow in unison in order to maintain the shape. It is worth noting that chain tilt in the usual sense did not develop at the beginning of the crystal growth—it is possible that the initial elliptic shape helps to avoid the frustration with the packing. Later on, when a larger central region with essentially flat thickness profile develops, the crystal obtains a tilt.

For a proper understanding of the crystal growth process, a clear picture of the kinetic barriers involved is needed. Incorporation of a new stem involves two steps. First, one of the transient stems with length below l_{min} at the growth front grows to a size larger than l_{min}, becoming stable and attached to the crystal. The process of a new stem growing larger than l_{min} (about 4 nm) is a fast one, as seen in Figure 4b, which shows that the stems reach that size in just tens of nanoseconds (the average growth rate of those small stems is still negative because so many of them shrink and disappear). This stage likely corresponds to the initial stage of linear growth for stems below 4 nm reported by Luo and Sommer.[13] In the second step, the stem grows with other stems toward l^* as new stems continue to attach (stabilize) at the growth front. The rate at which new stems attach was found to be related to l_{min}, suggesting that the free energy barrier for reaching the size l_{min} could be the rate-limiting factor and the subsequent growth a secondary process. A better understanding of these questions should be pursued in future work.

It is known that initial thickness of newly formed polymer crystals follows a relationship $l^* = l_c(T) + \delta l$, where $l_c \sim 1/\Delta T$ and δl is a constant. The "excess thickness" δl is independent of temperature and has a similar value in both melt and solution formed crystals.[11] This is quite remarkable, as the value then cannot depend on the mobility in the amorphous phase, but must follow from some intrinsic property. Here, the ultimate thickness of the crystal was found to be limited by the amount of slack length that is available for stem growth. The maximum length of a stem is therefore inversely proportional to the number of the stems in the chain, which in turn might conceivably be relatively independent of temperature or mobility in the amorphous phase. δl could therefore be determined by the statistics of how many stems form in crystalline chains relative to their length. As shown in Figure 4a, a large number of stems often form in a chain before any of them reach the full length l^*, which causes the average number of stems in a chain to be rather high.

Polyethylene crystals have been found to grow in thickness at sufficiently high temperatures even after their formation, indicating that a relaxation mechanism exists that allows the stems to grow further.[67] As chains with a large number of stems consitute a hindrance for thickening, a mechanism to reduce the number of stems in those chains should be identified. The mobile fold-against-fold defect shown in Figure 5 is such a mechanism, as it allows highly strained chains with lots of stems to reduce their number if a long enough amorphous segment is available to provide a new pair of stems. The formation of these defects at one fold surface and their migration to the other side leads to topological relaxation that could explain the observed crystal thickening.

CONCLUSION

We studied crystal growth in polyethylene with molecular dynamics in a large-scale system of 3 million united atoms with simulation times over 1 μs. We found new insights into both the edge region near the growth front and the central region where stem growth has slowed down. The edge region had a kinetically stable parabolic shape. The growth front is covered with a layer of short-lived transient stems that are too short to be stable. New stems are incorporated to the crystal when these stems reach a length over l_{min} and become stable. The attachment of new stems is accompanied by stem growth within the edge region, so as to maintain the parabolic shape. The temperature-dependent value of l_{min} seems to determine the crystal growth rate, i.e., the rate of stem attachment. These findings represent a step toward fuller understanding of polymer crystallization.

In the central region farther from the growth front, stem growth stalls because many chains lack the slack length necessary to grow the stems along their length. We discovered mobile crystal defects that can relax these constraints by

DOI: 10.1021/acs.macromol.8b00857
Macromolecules 2018, 51, 4865−4873

exchanging stems from a chain to another, leading to topological relaxation. These observations help to understand the initial crystal thickness selection and subsequent thickening observed experimentally in polyethylene.

AUTHOR INFORMATION

Corresponding Author

*E-mail tuukka.verho@vtt.fi; Tel +358 (0)40 5685783 (T.V.).

ORCID

Tuukka Verho: 0000-0003-1915-0845

Antti Paajanen: 0000-0002-4250-6363

Notes

The authors declare no competing financial interest.

ACKNOWLEDGMENTS

This work was supported by the Academy of Finland (Grant No. 289255).

REFERENCES

(1) Lin, L.; Argon, A. S. Structure and Plastic Deformation of Polyethylene. *J. Mater. Sci.* **1994**, *29*, 294−323.

(2) Patlazhan, S.; Remond, Y. Structural Mechanics of Semicrystalline Polymers Prior to the Yield Point: a Review. *J. Mater. Sci.* **2012**, *47*, 6749−6767.

(3) Galeski, A. Strength and Toughness of Crystalline Polymer Systems. *Prog. Polym. Sci.* **2003**, *28*, 1643−1699.

(4) Gedde, U. W.; Mattozzi, A. In *Long Term Prop. Polyolefins*; Mattozzi, A., Ed.; Springer: Berlin, 2004; pp 29−74.

(5) Strobl, G. Crystallization and Melting of Bulk Polymers: New Observations, Conclusions and a Thermodynamic Scheme. *Prog. Polym. Sci.* **2006**, *31*, 398−442.

(6) Strobl, G. Colloquium: Laws Controlling Crystallization and Melting in Bulk Polymers. *Rev. Mod. Phys.* **2009**, *81*, 1287−1300.

(7) Armitstead, K.; Goldbeck-Wood, G.; Keller, A. *Macromol. Synth. Order Adv. Prop.*; Springer: Berlin, 1992; pp 219−312.

(8) Muthukumar, M. Shifting Paradigms in Polymer Crystallization. *Lect. Notes Phys.* **2007**, *714*, 1−18.

(9) Hoffman, J.; Davis, J.; Lauritzen, J. In *Treatise on Solid State Chemistry*; Hannay, N. B., Ed.; Plenum: New York, 1976; pp 497−614.

(10) Hoffman, J. D.; Miller, R. L. Kinetic of Crystallization from the Melt and Chain Folding in Polyethylene Fractions Revisited: Theory and Experiment. *Polymer* **1997**, *38*, 3151−3212.

(11) Barham, P. J.; Chivers, R. A.; Keller, A.; Martinez-Salazar, J.; Organ, S. J. The Supercooling Dependence of the Initial Fold Length of Polyethylene Crystallized from the Melt: Unification of Melt and Solution Crystallization. *J. Mater. Sci.* **1985**, *20*, 1625−1630.

(12) Sadler, D. M.; Gilmer, G. H. A Model for Chain Folding in Polymer Crystals: Rough Growth Faces are Consistent with the Observed Growth Rates. *Polymer* **1984**, *25*, 1446−1452.

(13) Luo, C.; Sommer, J. U. Growth Pathway and Precursor States in Single Lamellar Crystallization: MD Simulations. *Macromolecules* **2011**, *44*, 1523−1529.

(14) Yamamoto, T. Molecular Dynamics of Polymer Crystallization Revisited: Crystallization from the Melt and the Glass in Longer Polyethylene. *J. Chem. Phys.* **2013**, *139*, 054903.

(15) Hu, W.; Cai, T. Regime Transitions of Polymer Crystal Growth Rates: Molecular Simulations and Interpretation Beyond Lauritzen-Hoffman Model. *Macromolecules* **2008**, *41*, 2049−2061.

(16) Jiang, X.; Reiter, G.; Hu, W. How Chain-Folding Crystal Growth Determines the Thermodynamic Stability of Polymer Crystals. *J. Phys. Chem. B* **2016**, *120*, 566−571.

(17) Sadler, D. M.; Gilmer, G. H. Rate-Theory Model of Polymer Crystallization. *Phys. Rev. Lett.* **1986**, *56*, 2708−2711.

(18) Sadler, D. M.; Gilmer, G. H. Selection of Lamellar Thickness in Polymer Crystal Growth: A Rate-Theory Model. *Phys. Rev. B: Condens. Matter Mater. Phys.* **1988**, *38*, 5684−5693.

(19) Sommer, J. U.; Reiter, G. Polymer Crystallization in Quasi-Two Dimensions. II. Kinetic Models and Computer Simulations. *J. Chem. Phys.* **2000**, *112*, 4384−4393.

(20) Luo, C.; Sommer, J. U. Coexistence of Melting and Growth During Heating of a Semicrystalline Polymer. *Phys. Rev. Lett.* **2009**, *102*, 147801.

(21) Sommer, J. U.; Luo, C. Molecular Dynamics Simulations of Semicrystalline Polymers: Crystallization, Melting, and Reorganization. *J. Polym. Sci., Part B: Polym. Phys.* **2010**, *48*, 2222−2232.

(22) Luo, C.; Sommer, J. U. Disentanglement of Linear Polymer Chains Toward Unentangled Crystals. *ACS Macro Lett.* **2013**, *2*, 31−34.

(23) Luo, C.; Sommer, J. U. Frozen Topology: Entanglements Control Nucleation and Crystallization in Polymers. *Phys. Rev. Lett.* **2014**, *112*, 1−5.

(24) Luo, C.; Sommer, J. U. Role of Thermal History and Entanglement Related Thickness Selection in Polymer Crystallization. *ACS Macro Lett.* **2016**, *5*, 30−34.

(25) Luo, C.; Kröger, M.; Sommer, J. U. Entanglements and Crystallization of Concentrated Polymer Solutions: Molecular Dynamics Simulations. *Macromolecules* **2016**, *49*, 9017−9025.

(26) Luo, C.; Kröger, M.; Sommer, J. U. Molecular Dynamics Simulations of Polymer Crystallization under Confinement: Entanglement Effect. *Polymer* **2017**, *109*, 71−84.

(27) Xiao, H.; Luo, C.; Yan, D.; Sommer, J. U. Molecular Dynamics Simulation of Crystallization Cyclic Polymer Melts As Compared to Their Linear Counterparts. *Macromolecules* **2017**, *50*, 9796−9806.

(28) Yamamoto, T. Molecular Dynamics Simulation of Polymer Crystallization Through Chain Folding. *J. Chem. Phys.* **1997**, *107*, 2653−2663.

(29) Yamamoto, T. Molecular Dynamics Modeling of Polymer Crystallization from the Melt. *Polymer* **2004**, *45*, 1357−1364.

(30) Yamamoto, T. Molecular Dynamics Simulations of Steady-State Crystal Growth and Homogeneous Nucleation in Polyethylene-like Polymer. *J. Chem. Phys.* **2008**, *129*, 184903.

(31) Yamamoto, T. Computer Modeling of Crystallization - Toward Computer-Assisted Materials' Design. *Polymer* **2009**, *50*, 1975−1985.

(32) Yamamoto, T. Molecular Dynamics of Reversible and Irreversible Melting in Chain-Folded Crystals of Short Polyethylene-like Polymer. *Macromolecules* **2010**, *43*, 9384−9393.

(33) Yamamoto, T. Molecular Dynamics in Fiber Formation of Polyethylene and Large Deformation of the Fiber. *Polymer* **2013**, *54*, 3086−3097.

(34) Paul, W.; Yoon, D. Y.; Smith, G. D. An Optimized United Atom Model for Simulations of Polymethylene Melts. *J. Chem. Phys.* **1995**, *103*, 1702−1709.

(35) Lavine, M. S.; Waheed, N.; Rutledge, G. C. Molecular Dynamics Simulation of Orientation and Crystallization of Polyethylene During Uniaxial Extension. *Polymer* **2003**, *44*, 1771−1779.

(36) Ko, M. J.; Waheed, N.; Lavine, M. S.; Rutledge, G. C. Characterization of Polyethylene Crystallization from an Oriented Melt by Molecular Dynamics Simulation. *J. Chem. Phys.* **2004**, *121*, 2823−2832.

(37) Waheed, N.; Ko, M. J.; Rutledge, G. C. Molecular Simulation of Crystal Growth in Long Alkanes. *Polymer* **2005**, *46*, 8689−8702.

(38) Yi, P.; Locker, C. R.; Rutledge, G. C. Molecular Dynamics Simulation of Homogeneous Crystal Nucleation in Polyethylene. *Macromolecules* **2013**, *46*, 4723−4733.

(39) Nicholson, D. A.; Rutledge, G. C. Molecular Simulation of Flow-Enhanced Nucleation in n-Eicosane Melts Under Steady Shear and Uniaxial Extension. *J. Chem. Phys.* **2016**, *145*, 244903.

(40) Balijepalli, S.; Rutledge, G. C. Molecular Simulation of the Intercrystalline Phase of Chain Molecules. *J. Chem. Phys.* **1998**, *109*, 6523−6526.

DOI: 10.1021/acs.macromol.8b00857
Macromolecules 2018, 51, 4865−4873

(41) Gautam, S.; Balijepalli, S.; Rutledge, G. C. Molecular Simulations of the Interlamellar Phase in Polymers: Effect of Chain Tilt. *Macromolecules* **2000**, *33*, 9136−9145.
(42) Lee, S.; Rutledge, G. C. Plastic Deformation of Semicrystalline Polyethylene by Molecular Simulation. *Macromolecules* **2011**, *44*, 3096−3108.
(43) Yeh, I.-C.; Andzelm, J. W.; Rutledge, G. C. Mechanical and Structural Characterization of Semicrystalline Polyethylene under Tensile Deformation by Molecular Dynamics Simulations. *Macromolecules* **2015**, *48*, 4228−4239.
(44) Yeh, I. C.; Lenhart, J. L.; Rutledge, G. C.; Andzelm, J. W. Molecular Dynamics Simulation of the Effects of Layer Thickness and Chain Tilt on Tensile Deformation Mechanisms of Semicrystalline Polyethylene. *Macromolecules* **2017**, *50*, 1700−1712.
(45) Liu, C.; Muthukumar, M. Langevin Dynamics Simulations of Early-Stage Polymer Nucleation and Crystallization. *J. Chem. Phys.* **1998**, *109*, 2536−2542.
(46) Muthukumar, M.; Welch, P. Modeling Polymer Crystallization from Solutions. *Polymer* **2000**, *41*, 8833−8837.
(47) Welch, P.; Muthukumar, M. Molecular Mechanisms of Polymer Crystallization from Solution. *Phys. Rev. Lett.* **2001**, *87*, 218302.
(48) Muthukumar, M. Molecular Modelling of Nucleation in Polymers. *Philos. Trans. R. Soc., A* **2003**, *361*, 539−556.
(49) Dukovski, I.; Muthukumar, M. Langevin Dynamics Simulations of Early Stage Shish-Kebab Crystallization of Polymers in Extensional Flow. *J. Chem. Phys.* **2003**, *118*, 6648−6655.
(50) Muthukumar, M. Modeling Polymer Crystallization. *Adv. Polym. Sci.* **2005**, *191*, 241−274.
(51) Gee, R. H.; Lacevic, N.; Fried, L. E. Atomistic Simulations of Spinodal Phase Separation Preceding Polymer Crystallization. *Nat. Mater.* **2006**, *5*, 39−43.
(52) Lacevic, N.; Fried, L. E.; Gee, R. H. Heterogeneous Directional Mobility in the Early Stages of Polymer Crystallization. *J. Chem. Phys.* **2008**, *128*, 014903.
(53) Hu, W. Chain Folding in Polymer Melt Crystallization Studied by Dynamic Monte Carlo Simulations. *J. Chem. Phys.* **2001**, *115*, 4395−4401.
(54) Hu, W.; Frenkel, D.; Mathot, V. B. Simulation of Shish-Kebab Crystallite Induced by a Single Prealigned Macromolecule. *Macromolecules* **2002**, *35*, 7172−7174.
(55) Hu, W.; Frenkel, D.; Mathot, V. B. Sectorization of a Lamellar Polymer Crystal Studied by Dynamic Monte Carlo Simulations. *Macromolecules* **2003**, *36*, 549−552.
(56) Ma, Y.; Hu, W.; Reiter, G. Lamellar Crystal Orientations Biased by Crystallization Kinetics in Polymer Thin Films. *Macromolecules* **2006**, *39*, 5159−5164.
(57) Hu, W.; Cai, T.; Ma, Y.; Hobbs, J. K.; Farrance, O.; Reiter, G. Polymer Crystallization Under Nano-Confinement of Droplets Studied by Molecular Simulations. *Faraday Discuss.* **2009**, *143*, 129.
(58) Wang, M.; Gao, H.; Zha, L.; Chen, E. Q.; Hu, W. Systematic Kinetic Analysis on Monolayer Lamellar Crystal Thickening via Chain-Sliding Diffusion of Polymers. *Macromolecules* **2013**, *46*, 164−171.
(59) Karayiannis, N. C.; Foteinopoulou, K.; Laso, M. Entropy-driven crystallization in dense systems of athermal chain molecules. *Phys. Rev. Lett.* **2009**, *103*, 045703.
(60) Karayiannis, N. C.; Foteinopoulou, K.; Abrams, C.; Laso, M. Modeling of Crystal Nucleation and Growth in Athermal Polymers: Self-Assembly of Layered Nano-Morphologies. *Soft Matter* **2010**, *6*, 2160−2173.
(61) Karayiannis, N. C.; Foteinopoulou, K.; Laso, M. The role of Bond Tangency and Bond Gap in Hard Sphere Crystallization of Chains. *Soft Matter* **2015**, *11*, 1688−1700.
(62) Foteinopoulou, K.; Karayiannis, N. C.; Laso, M. Monte Carlo Simulations of Densely-Packed Athermal Polymers in the Bulk and Under Confinement. *Chem. Eng. Sci.* **2015**, *121*, 118−132.
(63) Abraham, M. J.; Murtola, T.; Schulz, R.; Páll, S.; Smith, J. C.; Hess, B.; Lindahl, E. Gromacs: High Performance Molecular Simulations Through Multi-Level Parallelism from Laptops to Supercomputers. *SoftwareX* **2015**, *1*−*2*, 19−25.
(64) Ramos, J.; Vega, J. F.; Martínez-Salazar, J. Molecular Dynamics Simulations for the Description of Experimental Molecular Conformation, Melt Dynamics, and Phase Transitions in Polyethylene. *Macromolecules* **2015**, *48*, 5016−5027.
(65) Martin, M. G.; Siepmann, J. I. Transferable Potentials for Phase Equilibria. 1. United-Atom Description of n-Alkanes. *J. Phys. Chem. B* **1998**, *102*, 2569−2577.
(66) Auhl, R.; Everaers, R.; Grest, G. S.; Kremer, K.; Plimpton, S. J. Equilibration of Long Chain Polymer Melts in Computer Simulations. *J. Chem. Phys.* **2003**, *119*, 12718−12728.
(67) Reiter, G. Some Unique Features of Polymer Crystallisation. *Chem. Soc. Rev.* **2014**, *43*, 2055−2065.

DOI: 10.1021/acs.macromol.8b00857
Macromolecules 2018, 51, 4865−4873